Title
Ponytail motion

Author
Ding, Dingqian

Publication Date
2019

Peer reviewed|Thesis/dissertation

UNIVERSITY OF CALIFORNIA SAN DIEGO

Ponytail motion

A thesis submitted in partial satisfaction of the
requirements for the degree
Master of Science

in

Engineering Sciences (Mechanical Engineering)

by

Dingqian Ding

Committee in charge:

Professor Stefan G. Llewellyn Smith, Chair
Professor Padmini Rangamani
Professor David Saintillan

2019

The thesis of Dingqian Ding is approved, and it is acceptable in quality and form for publication on microfilm and electronically:

_____

_____

_____

Chair

University of California San Diego

2019

TABLE OF CONTENTS

LIST OF FIGURES

ACKNOWLEDGEMENTS

I would like to acknowledge Professor Stefan G. Llewellyn Smith for his support as the chair of my committee. He proposed this research project based on my research interests, and spent much time meeting with me to give useful suggestions to my thesis. His guidance has helped me learn to be a better researcher in the future.

I would also like to acknowledge Todd Christopher who gave me a lot of valuable advice for my thesis. Without him, my research would no doubt have taken much longer. His support helped me in immeasurable ways.

This thesis is co-authored with Dingqian Ding, Stefan G. Llewellyn Smith and Todd Christopher. The thesis author is the primary investigator and author of this material.

ABSTRACT OF THE THESIS

Ponytail motion

by

Dingqian Ding

Master of Science in Engineering Sciences (Mechanical Engineering)

University of California San Diego, 2019

Professor Stefan G. Llewellyn Smith, Chair

It is common knowledge that runners' ponytails will sway from side to side when running. This thesis treats the swaying phenomenon as a stability problem and discusses solution methods and results.

Geometrically nonlinear dynamical equations are derived for a flexible rod pointing vertically down and clamped at its base that is harmonically excited. Floquet theory is used to derive numerical methods to solve the problem. Results show the ponytail is always stable when it is unforced. When it is forced, it has a complex region of instability if it is treated as a flexible string, but that region becomes more limited if it is treated as a flexible rod. Adding different different types of damping can help dissipate the energy of the ponytail motion and further reduce

the instability region, so that for small enough forcing the motion is stable.

Chapter 1

Introduction

Vertically oriented vibrations of beams (clamped at the top and often free at the bottom) have many applications in industry such as stationary cranes and sub-sea flexible risers, and also many related applications in daily life, like fishing line on the fishing rod, tree swings and ponytail motion. Stability is one of the most important problems of vibration theory, and many researchers have treated the vertical motion of beams as pendulum vibrations: Plaut [1] treated a ponytail as a pendulum with one rigid bar or multiple rigid bars. However, these treatments are approximate, and some researchers have also directly investigated upside-down flexible rod (clamped at the bottom and free at the top). Champneys and Fraser [2] used Floquet theory and asymptotic analysis to investigate the stability of the Indian rope trick. Our interest in the stability of ponytail motion investigated by Keller [3] , which turns out to have important differences with the Indian rope trick.

Keller treated a ponytail as a rigid rod and then as a flexible string (see Figure 1.1), and took the acceleration of the head's motion to be small. This led to Hill's equation for the lateral motion of the ponytail. However, Keller did not investigate the stability region in detail, and he did not consider the cases when the acceleration of the head motion is large. Also, although Keller suggested investigating a model of the ponytail as an inextensible flexible rod with small

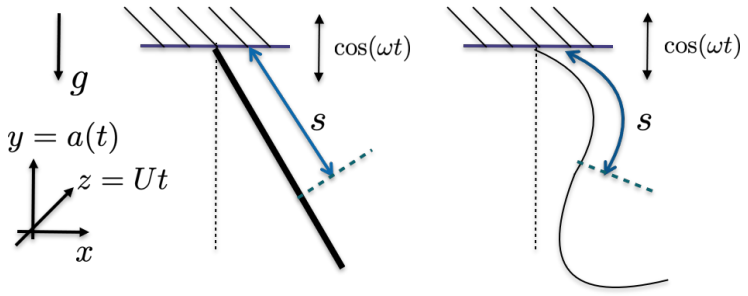

Figure 1.1: Sketch of rigid rod and flexible string.

bending stiffness, he did not provide the corresponding analysis.

However, the idea of Keller is interesting and this thesis will be based on Keller's paper. The goal is to investigate the stability of the oscillating flexible vertical rod problem, and to compare the results with the work of Champneys and Fraser[2]. Our goal is to discover the stability of the lateral displacement of ponytail motion, and understand the effect by different parameters. To do this we discuss the shape of ponytail and its normal modes, the frequency and amplitude of the head motion, the numerical methods that we use, and the stability regions for different situations.

The motion of a ponytail is one kind of parametrically excited system, and there are three traditional ways to investigate stability: Lyapunov methods, perturbation theory and Floquet theory. Lyapunov methods define a scalar function, the Lyapunov function, and uses derivative of that function to study stability of systems. Perturbation theory requires a small parameter to simplify the problem and obtain a manageable system. Floquet theory is a general approach for systems with periodic coefficients. It is hence appropriate for the stability analysis that follows.

1.1 Floquet theory

Consider a system of n linear differential equations of the form

$$\dot{x} = A(t)x \tag{1.1}$$

where $A(t)$ is a $n \times n$ periodic matrix function of time with period T. While solutions of the equation (1.1) are not necessarily periodic, at least one non-trivial solution $x(t)$ of equation (1.1) satisfies the following condition:

$$x(t+T) = \Lambda x(t), \tag{1.2}$$

where Λ is called the Floquet multiplier.

The general solution of the equation (1.1) can be written in the following form:

$$x_i = e^{\mu_i t} \tilde{X}_i(t) \tag{1.3}$$

where $e^{\mu T} = \Lambda$, and μ is called the Floquet exponent, which can be a complex number. There are two ways to use Floquet theory to obtain the stability regions. One way is the Floquet spectral method using Floquet exponents, and the other is the Floquet monodromy matrix method using Floquet multipliers.

For the Floquet spectral method, we need to solve for values of the Floquet exponents in equation (1.3) and determine whether the real parts of Floquet exponents $\mu = [\mu_1 \quad \mu_2 \quad ... \quad \mu_\infty]$ are smaller than 0 or not [4]. If one of the Floquet exponents has real part larger than 0, the system is unstable.

For the Floquet monodromy matrix method, we use linear independent solutions of the equation (1.1) to form a fundamental matrix $X(t) = [x_1(t), x_2(t), \ldots, x_n(t)]$. This fundamental matrix satisfies the equation

$$\dot{X} = AX, \tag{1.4}$$

X(T) is the monodromy matrix[5]. The eigenvalues of the monodromy matrix are the Floquet multipliers we need. Then we examine whether the absolute values of these Floquet multipliers are less than 1 or not. If one of them is larger than 1, the system is unstable. The numerical implementation of these two methods will be presented in Chapter 4.

In this thesis, Chapter 2 presents the mathematical model for the ponytail, Chapter 3 examines the stability and eigenfrequency of the unforced flexible rod problem, Chapters 4 and 5 use Floquet theory to find the stability regions of flexible string and flexible rod cases successively, and Chapter 6 considers the damped flexible rod problem. Finally Chapter 7 concludes.

Chapter 2

Mathematical Model of Ponytail

2.1 Mathematical formulation

Consider a runner's ponytail as an inextensible flexible rod with small bending stiffness B, constant density ρ and length L. The ponytail is clamped at one end and free on the other. Assume the runner runs along the z axis with constant speed U, and the ponytail moves up and down with his head in the y axis with displacement $a(t)$ (see Figure 2.1).

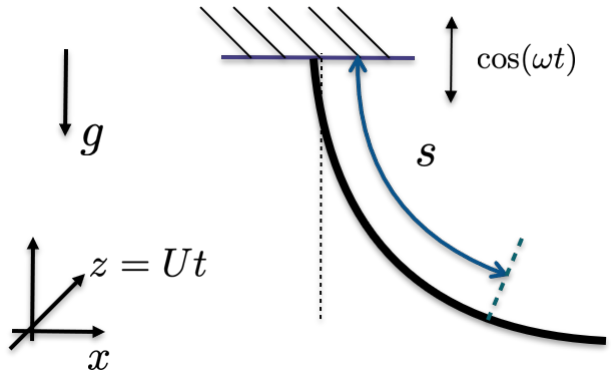

Figure 2.1: Sketch of flexible rod.

Let $\mathbf{x} = (x(s,t), y(s,t))$ be the displacement of the ponytail at time t. It can be shown that

it satisfies the equation

$$\rho \mathbf{x}_{tt} = (T\mathbf{x}_s)_s + \rho g - B\mathbf{x}_{ssss}, \quad 0 < s < L \tag{2.1}$$

where $T(s,t)$ is the tension of the rod that is obtained as part of the solution.

Following Keller, consider the ponytail in equilibrium

$$\mathbf{x}^0(s,t) = [0, a(t) - s]. \tag{2.2}$$

The corresponding tension $T^0(s,t)$ can be integrated with respect to s, and satisfies free condition at $s = L$, namely $T(L,t) = 0$. We find

$$T^0(s,t) = \rho(g + a_{tt})(L - s). \tag{2.3}$$

After linearizing the problem around this solution, the equation for the x- displacement $x(t)$ becomes

$$\rho x_{tt} = \rho(g + a_{tt})[(L - s)x_s]_s - Bx_{ssss}, \quad 0 < s < L. \tag{2.4}$$

Since the ponytail is clamped at the top and free at the bottom, we obtain the following boundary conditions

$$x(0,t) = 0, \quad x_s(0,t) = 0, \quad x_{ss}(L,t) = 0, \quad x_{sss}(L,t) = 0. \tag{2.5}$$

This means that both deflection and slope are zero at the top, and the bending moment and the shear force are zero at the bottom.

2.2 Dimensionless model

In order to simplify the equation we define, define dimensionless variables as follows:

$$s^* = \frac{s}{L}, \qquad x^* = \frac{x}{L}, \qquad t^* = \omega t, \qquad a(t)^* = a(t)/A, \tag{2.6}$$

where A is the amplitude of the excitation and ω is the typical angular frequency of the excitation.

When (2.6) is substituted into (2.4), the result is

$$x^*_{t^*t^*} = \left(\frac{g}{L\omega^2} + \frac{Aa^*_{t^*t}}{L}[(1-s^*)x^*_s]_{s^*} \right) - \frac{Bx_{s^*s^*s^*s^*}}{\rho L^4 \omega^2} \tag{2.7}$$

Drop * from now on, and define using the following dimensionless variables

$$\delta = \frac{g}{L\omega^2}, \qquad \varepsilon = \frac{A}{L}, \qquad B^* = \frac{B}{\rho g L^3}. \tag{2.8}$$

Then the governing equation finally becomes

$$x_{tt} = (\delta + \varepsilon a_{tt})[(1-s)x_s]_s - \delta B x_{ssss}. \tag{2.9}$$

We have taken the time-dependent forcing in (2.9) to be purely harmonic so that $a_{tt} = \cos t$, and we will use this forcing throughout the thesis. As the boundary conditions are homogeneous, they are unchanged and take the form

$$x(0,t) = 0, \quad x_s(0,t) = 0, \quad x_{ss}(1,t) = 0, \quad x_{sss}(1,t) = 0. \tag{2.10}$$

Chapter 3

The unforced problem

In this chapter, we consider the ponytail as flexible rod without external forces, as we want to study the stability and natural frequencies of this unforced problem when $\varepsilon = 0$ in the equation (2.9). The governing equation becomes

$$x_{tt} = \delta[(1-s)x_s]_s - \delta B x_{ssss}. \tag{3.1}$$

We use separation of variables to find normal modes (this method will also be used in chapter 4), and the corresponding eigenvalues provide the natural frequencies of the rod.

3.1 Normal-mode calculation

Equation (3.1) can be solved by the method of separation of variables. The solution takes the form

$$x(s,t) = \sum_{n=1}^{\infty} \phi_n(s)(A_n \cos \omega_n t + B_n \sin \omega_n t), \tag{3.2}$$

with

$$A\phi_n(s) - \lambda_n \phi_n(s) \equiv B\phi_n''''(s) - [(1-s)\phi_n(s)']' - \lambda_n \phi_n(s) = 0, \tag{3.3}$$

where $\phi_n(s)$ are the eigenfunctions satisfying the boundary conditions (2.10) with $\phi_n(1)$ normalized to equal one, λ_n are the eigenvalues, and ω_n are the natural angular frequencies, with $\lambda_n = \omega_n^2/\delta$. The eigenfunctions satisfy the orthogonality condition, which can been proved as follows.

We take any two eigenfunctions satisfying

$$B\phi_n(s)'''' - [(1-s)\phi_n(s)']' - \lambda_n\phi_n(s) = 0, \tag{3.4}$$

$$B\phi_m(s)'''' - [(1-s)\phi_m(s)']' - \lambda_m\phi_m(s) = 0, \tag{3.5}$$

multiply equation (3.4) by ϕ_m and multiply equation (3.5) by ϕ_n to get

$$B\phi_n(s)''''\phi_m(s) - [(1-s)\phi_n(s)']'\phi_m(s) - \lambda_n\phi_n(s)\phi_m(s) = 0, \tag{3.6}$$

$$B\phi_m(s)''''\phi_n(s) - [(1-s)\phi_m(s)']'\phi_n(s) - \lambda_m\phi_m(s)\phi_n(s) = 0. \tag{3.7}$$

Then subtract equation (3.6) from equation (3.7) to get

$$\underbrace{B(\phi_m(s)''''\phi_n(s) - \phi_n(s)''''\phi_m(s))}_{\text{First term}} - \underbrace{([(1-s)\phi_m(s)']'\phi_n(s) - [(1-s)\phi_n(s)']'\phi_m(s))}_{\text{Second term}} - \underbrace{\phi_m(s)\phi_n(s)(\lambda_m - \lambda_n)}_{\text{Third term}} = 0. \tag{3.8}$$

Integrate the above equation from 0 to 1 and use integration by parts. The remaining term will be

$$\int_0^1 \phi_m(s)\phi_n(s)(\lambda_m - \lambda_n) = (\lambda_m - \lambda_n)\int_0^1 \phi_m(s)\phi_n(s) = 0. \tag{3.9}$$

Therefore we get

$$\int_0^1 \phi_n(s)\phi_m(s)ds = N_n\delta_{nm}, \tag{3.10}$$

where $N_n = \int_0^1 \phi_n^2(s)ds$ and δ_{nm} is the Kronecker delta. Now we need to solve (3.3). As our boundary conditions are non-periodic, we use a Chebyshev spectral method to discretize in space.

3.2 Chebyshev spectral method

The Chebyshev spectral method is one kind of spectral collocation methods that can be used to solve non-periodic boundary value problems. It introduces Chebyshev points ($x_j = \cos(j\pi N)$, $j = 0, 1, \ldots, N$) and uses the Lagrange Interpolating Polynomial to construct Chebyshev differentiation matrices (see below). One can then use these matrices to construct linear algebra analogs of the ordinary differential equations.

The Lagrange Interpolating Polynomial is the polynomial $P(x)$ of degree $\leq N$ that passes through the n points (x_1, v_1), ..., (x_n, v_n). It takes the form

$$P(x) = \sum_{j=1}^{n} P(x_j), \tag{3.11}$$

where

$$P(x_j) = v_j \prod_{\substack{k=1 \\ k \neq j}}^{N} \frac{x - x_k}{x_j - x_k}. \tag{3.12}$$

If one writes $w_j = P'(x_j)$, as this operation is linear, $w = D_N v$, where D_N is $(N+1) \times (N+1)$ matrix, which takes the form [6]:

$$(D_N)_{00} = \frac{2N^2 + 1}{6}, \qquad (D_N)_{NN} = -\frac{2N^2 + 1}{6}, \tag{3.13}$$

$$(D_N)_{jj} = \frac{-x_j}{2(1 - x_j^2)}, \qquad j = 1, \ldots, N-1, \tag{3.14}$$

$$(D_N)_{ij} = \frac{c_i}{c_j} \frac{(-1)^{i+j}}{x_i - x_j}, \qquad i \neq j, \quad i, j = 1, \ldots, N-1, \tag{3.15}$$

where

$$c_i = \begin{cases} 2 & i = 0, N \\ 1 & \text{otherwise} \end{cases} \tag{3.16}$$

Here we use the MATLAB function `cheb` from Trefethen's book [6]. This function returns

Chebyshev grids and Chebyshev differentiation matrix.

After obtaining the Chebyshev differentiation matrix, we need to apply the boundary conditions to this matrix. This discussion is not standard. The basic idea is, as these four boundary conditions are all homogeneous, we can write them as a matrix, C with

$$Cx = 0 \tag{3.17}$$

where

$$C = \begin{pmatrix} zeros(1,N) & 1 \\ D_N(N+1,:) \\ D_N^2(1,:) \\ D_N^3(1,:) \end{pmatrix},$$

to satisfy the boundary conditions (2.10). The null-space matrix

$$U = null(C), \tag{3.18}$$

provides an orthonormal basis for the null space of C, and if limit x to its range, we will construct solutions that satisfy (2.10).

As the eigenvalue problem (3.3) can be written after discretization as a linear eigenvalue problem

$$Ax = \lambda x, \tag{3.19}$$

we take $x_* = U^T x,\ A_* = U^T AU$ to project x and A onto the null space. Then

$$A_* x_* = \lambda x_*, \tag{3.20}$$

After this transformation, we can use the MATLAB function `eig` to obtain the eigenvalues and discretized eigenfunctions.

3.3 Eigenfrequencies and stability

This section discuss the natural frequencies and stability of the unforced problem. Before solving the eigenproblem with the Chebyshev spectral method, we need to compare the accuracy of different numbers of Chebyshev points, and choose a large enough number of gridpoints to obtain adequate accuracy.

3.3.1 Accuracy of Chebyshev spectral method

When $B = 0$, (3.3) has an exact solution, which is expressed in terms of the Bessel function J_0:

$$\phi_n(s) = J_0[2\lambda_n^{1/2}(1-s)^{1/2}], \qquad \lambda_n = j_n^2/4, \tag{3.21}$$

where $j_n, n = 1, 2, \ldots$ is the infinite increasing sequence of positive roots of the Bessel function J_0, and the boundary conditions satisfied are

$$\phi_n(0) = 0, \quad \phi_n(1) = \text{finite}. \tag{3.22}$$

After getting the exact solution, we use the Chebyshev spectral method to solve eigenvalue problem (3.3) with $B = 0$. Figure 3.1 shows the error when comparing the value of first, fifth and twentieth eigenvalues. We can see that the numbers of Chebyshev points needed increases with the eigenvalue. Therefore, as we keep 5 eigenvalues for this chapter's calculation, we choose 50 Chebyshev points for accuracy.

3.3.2 Discussion

Figure 3.2(a) and (b) show the shapes of the eigenfunctions for the first five eigenvalues $\lambda_n = \omega_n^2/\delta$, when $B = 0.001$ and $B = 1$. Figure 3.2 (c) and (d) show the locus of the eigenfrequencies and eigenvalues as functions of B, again for the first five eigenfunctions.

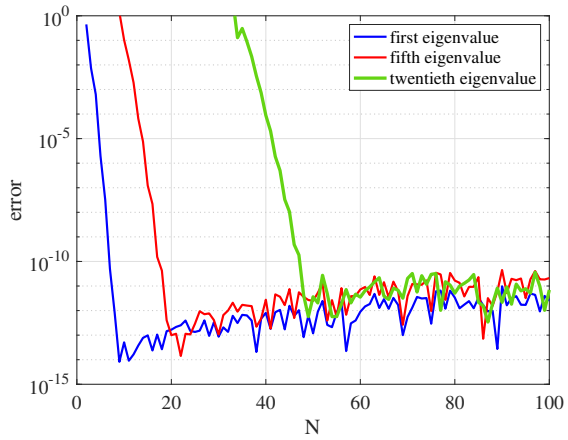

Figure 3.1: The error of the first three eigenvalues calculated by the Chebyshev Spectral method applied to (3.1) when $B = 0$ computed for different numbers of collocation points.

The first step is to investigate the eigenfrequency of this unforced problem. Figure 3.2(a)(b) show the eigenfunctions for different values of B. The frequencies are small when B is small. Figure 3.2(a) and (b) are similar to Figure 2(a) of Champneys and Fraser[2], but there is a critical difference in the stability properties, as we now discuss.

The next step is to examine the stability of this unforced problem. Figure 3.2 (d) show that all of eigenvalues are positive, Hence $x(s,t)$ is bounded value, so small displacement from the vertical position will result in bounded lateral oscillations of the ponytail. This is not surprising since the ponytail hangs down. This result is quite different from the paper of Champneys and Fraser[2], as in their problem, the Indian rope trick has unstable regions when it is unforced. Physically, the Indian rope trick consists of an upside-down column: if it does not have high enough bending stiffness or is not very short length, it is easily be buckled. For our problem, the ponytail can be unstable only when it is forced.

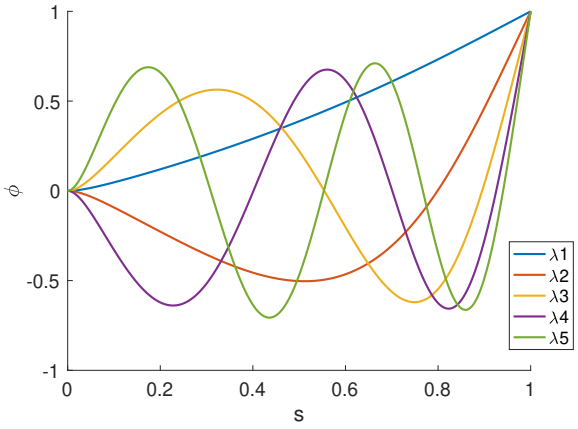

(a) Eigenfunctions for $B = 0.001$.

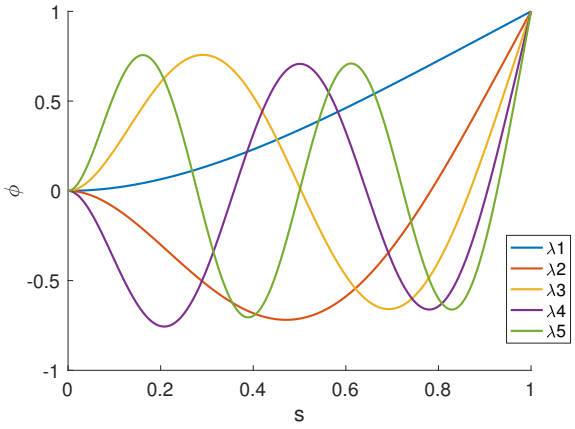

(b) Eigenfunctions for $B = 1$.

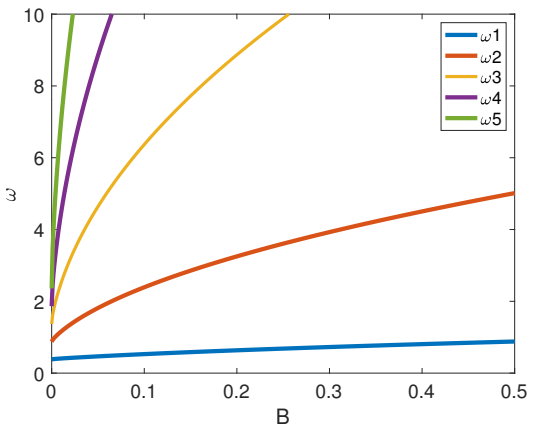

(c) Loci of the eigenfrequencies as function of B.

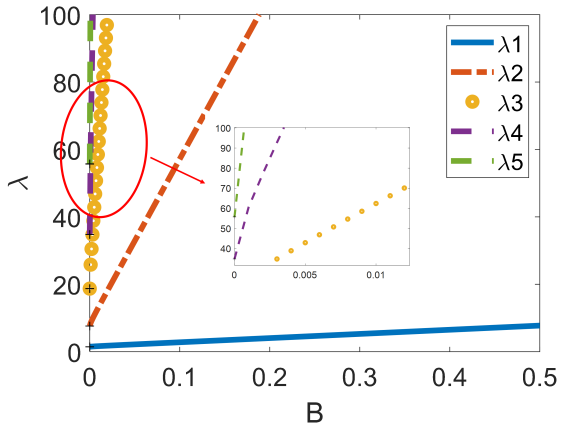

(d) Loci of the eigenvalues as function of B.

Figure 3.2: Relations among eigenfunction, bending stiffness, eigenvalues and natural frequencies.

Chapter 4

The string problem

In this chapter, we investigate the forced string problem. This study is based on Keller's paper and lays the foundation for the flexible rod problem in the next chapter.

4.1 Solution by separation of variables

When we consider the string problem, the equation (2.9) becomes the second-order differential equation

$$x_{tt} = (\delta + \varepsilon a_{tt})Mx, \quad M = [(1-s)_s]_s, \quad 0 < s < 1, \tag{4.1}$$

where $a_{tt} = \cos t$. As this is a second-order differential equation, it needs two boundary condition. The string is clamped at the top and free at the bottom, so the boundary conditions are

$$x(0,t) = 0, \quad x(1,t) = \text{finite}, \quad 0 < s < 1. \tag{4.2}$$

(Note the difference with the rod problem which has four boundary conditions.)

This problem can still solved by the method of separation of variables. The solution and

corresponding eigenfunctions take the form

$$x(s,t) = \sum_{n=1}^{\infty} \phi_n(s) u_n(t), \tag{4.3}$$

and

$$-M\phi_n - \lambda_n \phi_n \equiv -\left[(1-s)\phi_n^{'}\right]^{'} - \lambda_n \phi_n = 0. \tag{4.4}$$

Plugging equation (4.3) and (4.4) into equation (4.1), we obtain

$$\sum_{n=1}^{\infty} (u_n''(t) + (\lambda_n \delta + \lambda_n \varepsilon \cos t) u_n(t)) \phi_n(s) = 0. \tag{4.5}$$

The eigenfunctions ϕ_n can be expressed in terms of the Bessel function J_0 as explained in equation (3.21), and therefore the eigenfunctions are orthogonal. The equation (4.5) becomes

$$u_n''(t) + (\lambda_n \delta + \lambda_n \varepsilon \cos t) u_n(t) = 0, \tag{4.6}$$

which represents an infinite number of Mathieu equations. In equation (4.6), the parameters ε and δ are multiplied by λ_n. Both increase as n increases, but the ratio ε/δ remains constant (as these two nondimensional numbers are $\delta = g/L\omega^2$ and $\varepsilon = A/L$). As we want to derive stability regions in terms of these two non-dimensional numbers, we treat all the points $(\lambda_n\delta, \lambda_n\varepsilon)$ move along the lines with the slope of ε/δ. Then $\lambda_n\delta$ and $\lambda_n\varepsilon$ in equation (4.6) can be rescaled as $\delta^* = \lambda_n\delta$ and $\varepsilon^* = \lambda_n\varepsilon$, and we obtain the simple Mathieu equation

$$u_n''(t) + (\delta^* + \varepsilon^* \cos t) u_n(t) = 0. \tag{4.7}$$

Figure 4.1 shows the stability region of the Mathieu equation solved by the Floquet monodromy matrix method (the method is discussed in the next section). The lines show the five lowest points $\lambda_n(\delta, \varepsilon)$ corresponding to the parameters in the infinite number of Mathieu equations

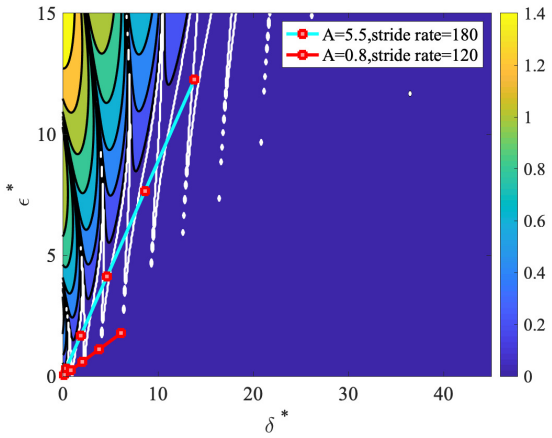

Figure 4.1: Stability regions for equation (4.7) with scaled axes.

when people is walking and running (the details of this example are discussed in section 4.3). The core idea of this rescaling is to turn the question of stability of the string into the question of whether any of the infinite number of points $\lambda_n(\delta,\varepsilon)$ lie in a region of instability.

4.2 Numerical Method

The equation (4.7) can be solved by the Floquet methods outlined in the Introduction. This section presents the two approaches.

4.2.1 Floquet monodromy matrix method

For the Floquet monodromy matrix method, we need to rewrite the equation (4.7) in the form $\dot{X} = AX$, which here becomes

$$\begin{pmatrix} \dot{u}_0 \\ \dot{u}_1 \end{pmatrix} = \begin{pmatrix} 0 & 1 \\ -(\delta^* + \varepsilon^* \cos t) & 0 \end{pmatrix} \begin{pmatrix} u_0 \\ u_1 \end{pmatrix}, \tag{4.8}$$

where $u_0 = u$ and $u_1 = \dot{u}$. Using $u(0) = I$ as initial condition, where I is the 2×2 identity matrix, we find the monodromy matrix $u(T)$ with $T = 2\pi$.

We use the Matlab ODE solver to solve the systems of ODEs. As this problem is not stiff, here we use ode45 and ode 113 to solve and compare the accuracy and efficiency of these two ODE Solver. The algorithm of ode45 is an explicit Runge-Kutta (4,5) formula, which has medium accuracy, while ode113 is a variable-step, variable-order (VSVO) Adams-Bashforth-Moulton PECE solver of orders 1 to 13, which is more efficient than ode45 at problems with stringent error tolerances [7]. For this problem, we keep the relative tolerance at 10^{-8} and absolute tolerance at 10^{-10} in both ODE solvers. The computation domain is 45×15 with 600 grid points in δ direction and 200 grid points in ε direction. The results are shown in Figure 4.2. They have been converted from Floquet multipliers to Floquet exponents using the relation $e^{\mu T} = \Lambda$ to compare the result of two Floquet methods. The results agree with the known stability boundaries for the Mathieu equation. Both ode45 and ode 113 reproduce the stability boundary defined by a value of 10^{-8} (see Figure 4.2. The routine ode113 solves over 1000 seconds faster than ode 45, but we see examine Figure 4.2(b), we find that the result of ode 113 has lots of black regions. These regions are at the level of 10^{-10}, and show that ode 113 does not solve very accurately. Therefore, although ode113 solves faster than ode45, in order to keep accuracy, we need to choose ode45 in the rest of thesis.

4.2.2 Floquet Spectral method

As discussed in the Introduction, the general solution for u can be written as

$$u = e^{\mu T}\tilde{U}(t), \tag{4.9}$$

where $\tilde{U(t)}$ can be expanded as a Fourier series with period $T = 2\pi$:

$$\tilde{U}(t) = \sum_{n=-\infty}^{\infty} U_n e^{int}. \tag{4.10}$$

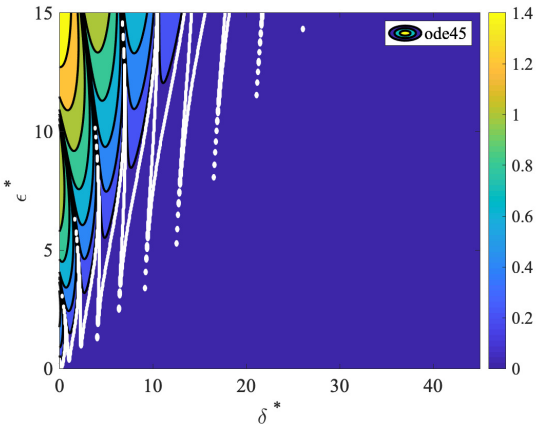

(a) Solving with MATLAB ode45.

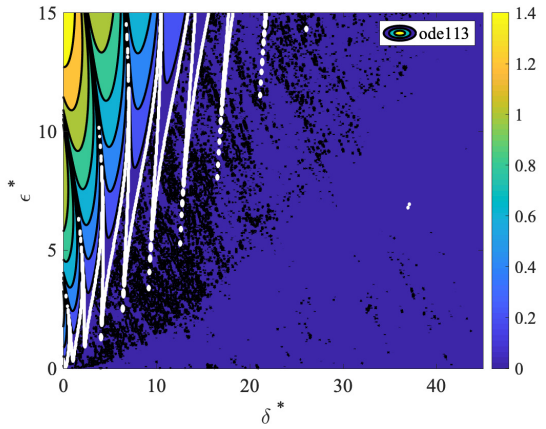

(b) Solving with MATLAB ode113.

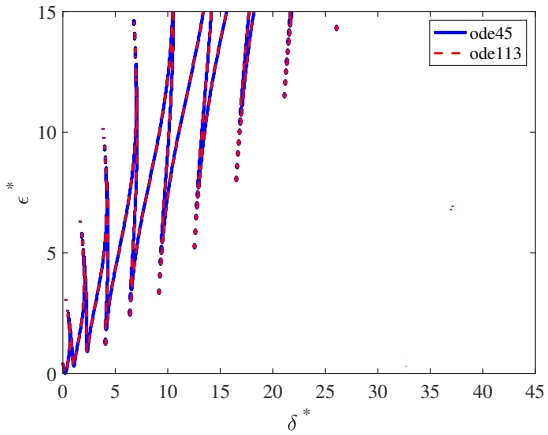

(c) Comparison of the boundary of these two ODE Solver.

Figure 4.2: Comparison of the results of ODE Solver in Floquet monodromy matrix method: ode45 and ode113.

Therefore, the equation 4.7 can be transformed into

$$\sum_{n=-\infty}^{\infty} -n^2 U_n + (\delta^* + \varepsilon^* \cos t) \sum_{n=-\infty}^{\infty} U_n + \mu(\sum_{n=-\infty}^{\infty} 2inU_n) + \mu^2 \sum_{n=-\infty}^{\infty} U_n = 0. \tag{4.11}$$

As it is impossible to use infinity numbers of terms in the Fourier series, the sum $\sum_{-\infty}^{\infty} U_n$ needs to be truncated with enough terms in $\sum_{-N}^{N} U_n$ to ensure accuracy. Then equation (4.11) can be

written as

$$(D+\mu E+\mu^2 F)\begin{pmatrix} U_{-N} \\ U_{-N+1} \\ \vdots \\ U_{N-1} \\ U_N \end{pmatrix} = 0 \tag{4.12}$$

where

$$D = \begin{pmatrix} -(-N)^2+\delta^* & \frac{\varepsilon^*}{2} & 0 & \dots & \dots \\ \frac{\varepsilon^*}{2} & -(-N+1)^2+\delta^* & \frac{\varepsilon^*}{2} & \dots & \dots \\ 0 & \ddots & \ddots & \ddots & \\ \vdots & & \frac{\varepsilon^*}{2} & -(N-1)^2+\delta^* & \frac{\varepsilon^*}{2} \\ 0 & \dots & \dots & \frac{\varepsilon^*}{2} & -(N)^2+\delta^* \end{pmatrix}$$

$$E = \begin{pmatrix} 2i(-N) & 0 & \dots \\ 0 & 2i(-N+1) & \dots \\ \vdots & \ddots & \\ 0 & \dots & 2i(N) \end{pmatrix}$$

$$F = \begin{pmatrix} 1 & 0 & \dots \\ 0 & 1 & \dots \\ \vdots & \ddots & \\ 0 & \dots & 1 \end{pmatrix}$$

Equation (4.12) is a polynomial eigenvalue problem, and we use the Matlab `polyeig` function to find the Floquet exponents, and see whether the real parts of these Floquet exponents are smaller than zero or not. However, as Turhan pointed out in [4], it is necessary to introduce

constraints on the imaginary parts of the Floquet exponents to remove the indefiniteness and produce unique Floquet exponents. For our case, we require $0 \leq |\mathrm{Im}(\mu)| \leq 1$. Then from Figure 4.2(a) we find the result using five Fourier terms is close enough to that with ten terms. Hence five Fourier modes is enough for this case. In addition the result with five Fourier terms has same stability region as the result of solving with the Floquet monodromy matrix method (see Figure 4.2(b)). As a result both of these two methods could be used in the following sections. We note that the Floquet Spectral method is more efficient than the Floquet monodromy matrix method when solving equation 4.7 on a 5×5 computational domain with 200 grid points in the δ-direction and 200 grid points in the ε-directions. The Floquet Spectral method takes 15 seconds to solve this problem, however, the Floquet monodromy matrix method takes 360 seconds. Therefore, the Floquet Spectral method will be the first choice for the following computation.

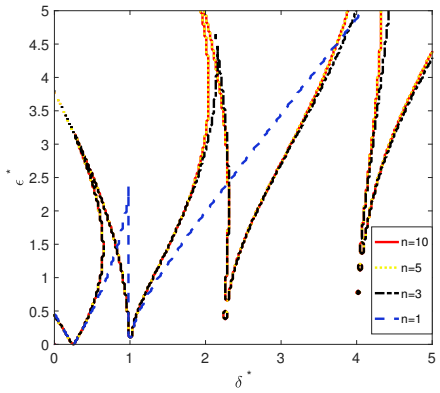

(a) Solving equation 4.7 with Floquet spectral method, and comparing results of different Fourier modes.

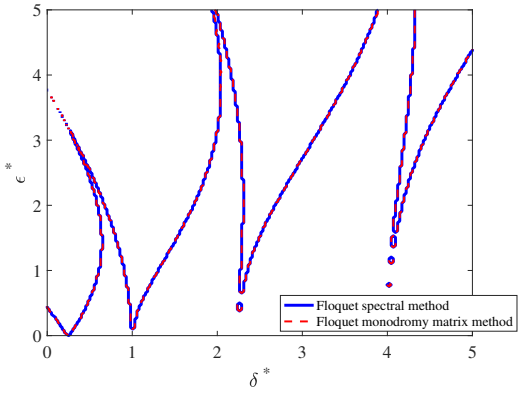

(b) Comparison of results of Floquet monodromy matrix method with Floquet Spectral method with same computational domain.

Figure 4.3: Comparison of the results of the two Floquet methods.

4.3 Stability Regions

In this section we will examine the stability regions for the flexible string using the two Floquet methods and discuss the stabilities of the ponytail with different stride rates.

Solving equation 4.7 again and setting 600 grid points in the δ-direction and 200 grid points in the ε-direction within 45×15 computational domain. For the Floquet monodromy matrix method, we take the relative error to be less than 10^{-8} and absolute error less than 10^{-10}. For the Floquet Spectral method, we choose $N = 8$ modes in Fourier series. We have transformed the result of the Floquet monodromy matrix method to the form of Floquet exponents. As seen in the Figure 4.4, the stability regions are the same.

Following the idea of section 4.1, the way we find whether the ponytail of people is stable or unstable is by using the infinite number of points $\lambda_n(\delta, \varepsilon)$ to see if these points lie in a region of instability. The two lines in figure 4.4 show two kinds of conditions: the blue line corresponding to people walking, and the red line corresponding to people running. The first five $\lambda_n(\delta, \varepsilon)$ points are shown. The information is given by the paper of Takahashi et al. [8]. They carried out experiments and found that the frequency of head movement in the vertical direction for normal walking and running were 2 and 3 Hz (= 2 and 3 cycles/s = 4π and 6π rad/s). In order to match the frequency of head motion to stride rates, we assume a cycle is equal to a step with one leg, so 2 and 3 cycles/s correspond to 120 and 180 cycles/minute, i.e. 120 and 180 steps/minute. However, when we calculate the values of δ and ε, we need to use the unit of radians/sec . That paper also shows that vertical head displacement are 0.8 ± 0.3 cm when people are walking and 5.5 ± 1.3 cm when people are running, so we choose $A = 0.8$ and $A = 5.5$ for walking and running respectively.

The two dimensionless numbers $\delta = g/L\omega^2$ and $\varepsilon = A/L$ are related to the vertical head displacement (A), length of ponytail (L), and pace (ω). We set the length of ponytail to be 25 cm, and set the other valuables from [8]. The way to calculate λ_n has been described in section 4.1. It

seems that the first points $\lambda_1(\delta,\varepsilon)$ are clustered in the first and second instability regions, which means if these points are really in the first and second regions of instability, we do not need to check any further. Therefore, we set the enough numbers of points $\lambda_n(\delta,\varepsilon)$, and check points by points until they are in unstable regions or the calculation is over. After comparing these two lines, we can conclude that if the slope of ε/δ is larger, the ponytail will be more likely to be in unstable regions. That is why we often see the ponytail sways side to side when people are running and seldom see this phenomenon when people are walking. (The small black points in Figure 4.4(a) is the error of Floquet Spectral method, which is at the level of 10^{-16}, and can be ignored.)

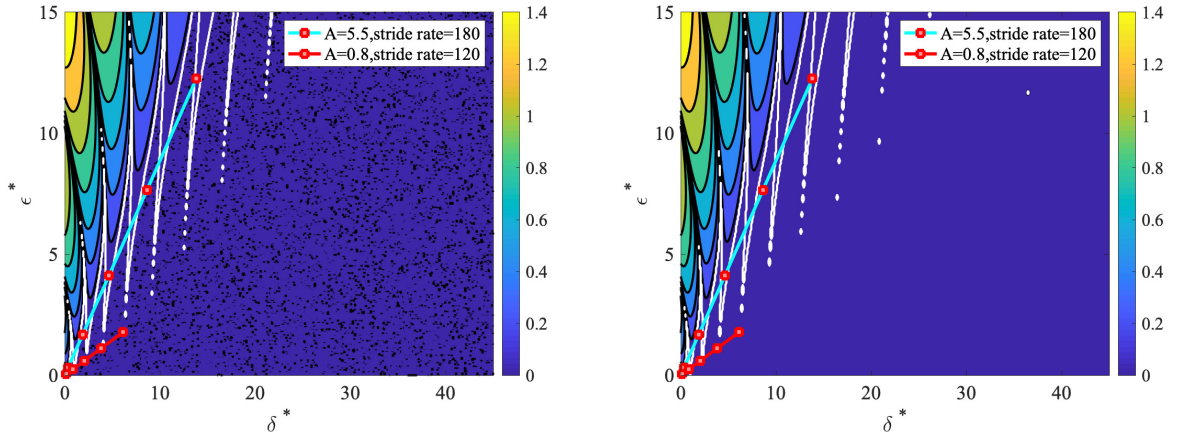

(a) Stability of ponytail when people are walking (red line) or running (blue line) (using the Floquet spectral approach).

(b) Stability of ponytail when people are walking (red line) or running (blue line) (using the Floquet monodromy matrix).

Figure 4.4: Comparison of the results of these two methods.

4.4 Discussion

For the flexible string problem, using the method of separation of variables is one way to ease the problem (see the equation 4.7). However, for the flexible rope problem in the next chapter, we can no longer use the method of separation of variables to solve the equation. Hence

we present here another way to solve the flexible string problem, using the Chebyshev Spectral method to discretize the space and using either Floquet approach. We then compare the results of these two methods to ensure both are accurate.

4.4.1 Compiling results from the method of separation of variables

In section 4.3, we use an infinite number of points $\lambda_i(\delta,\varepsilon)$ to examine if these points lie in unstable regions of Mathieu's equation. Here, in order to compare with the next method of fully discretization of equation (4.1), we assemble results using a large number of eigenvalues (λ_i from $i = 5$ to 50) and obtain the largest Floquet exponents from these results to ensure that every grid point in computational domain has been accurately computed. (As the Floquet Spectral method is more efficient than the Floquet monodromy matrix method, we use the Floquet Spectral method in this section).

In Figure 4.5(e), we set 200 points in both the δ and ε directions within 1×1 computational domain (as both δ and ε is smaller than 1 in real case), and it shows the stability regions with 5 to 50 eigenvalues, and the stability boundary does not change when we choose 35 eigenvalues. However, we are concerned about whether the grid numbers are enough to capture all resonance tongues. Therefore, we add more grid points and just see what happens for region of stability within the small-δ region with more eigenvalues. Figures 4.5(a)–(d) use 500 points in both the δ and ε directions, and we find that when we increase the number of eigenvalues, more resonance regions appear. Then, we compare the result of Figures 4.5c) and (d): though the number of resonance tongues seems not to change, the values of the Floquet exponents continually grows when δ is small. This means that although Figure 4.5(c) and (d) look quite similar, we believe if we add more grid points we can see more tiny resonance tongues. This appears to be why the values of Floquet exponents become large as we add more eigenvalues. Physically the flexible string could have an infinite number of unstable resonant regions as it does not have bending stiffness.

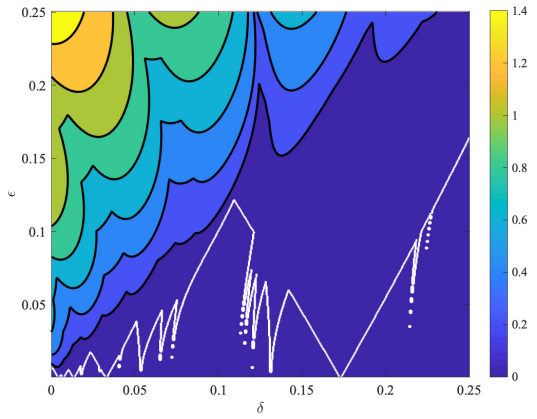

(a) 5 eigenvalues.

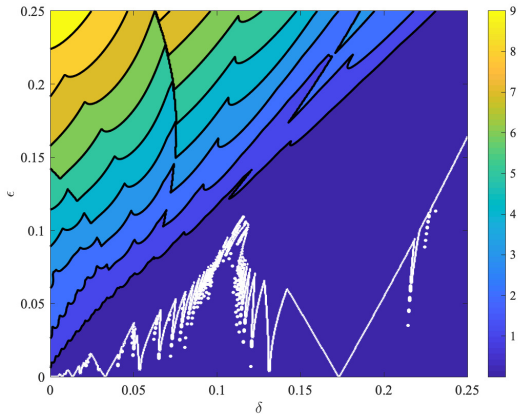

(b) 20 eigenvalues.

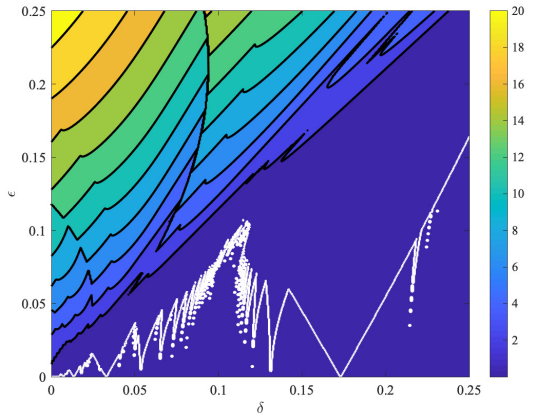

(c) 35 eigenvalues.

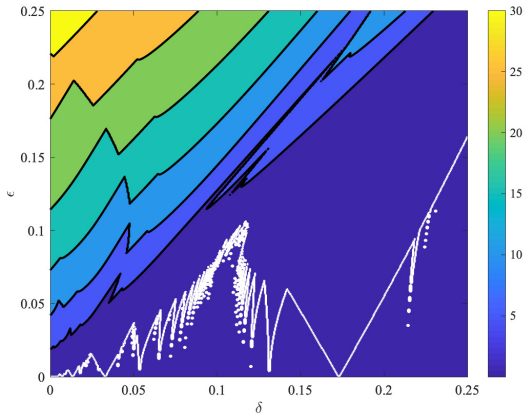

(d) 50 eigenvalues.

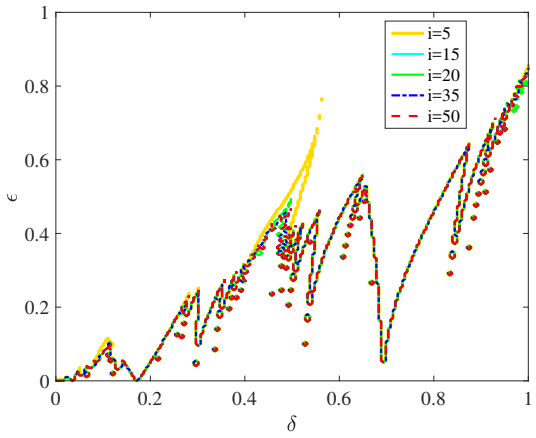

(e) 5, 15, 20, 35 and 50 eigenvalues.

Figure 4.5: Compiling results from the method of separation method with different eigenvalues.

4.4.2 Spatial problem

After obtaining results using the method of separation of variables, the next thing is to turn the problem into a spatial problem and use Chebyshev Spectral method to discretize in space equation (4.1). It then becomes

$$x_{tt} = (\delta + \varepsilon a_{tt})Mx, \quad M = [(1-s)D_K]D_K, \quad 0 < s < 1, \tag{4.13}$$

where D_K is the Chebyshev differentiation matrix with K Chebyshev modes. After discretizing the equation, we need to investigate convergence first and then verify accuracy.

In Figure 4.6, we still set 200 points in both the δ and ε directions within 1×1 computational domain and directly discretize equation (4.1). First, we fix the number of Chebyshev points to 10, and vary the Fourier modes. We see in Figure 4.6 that the stability regions are unchanged when the number of Fourier modes is 15. Then, we take 15 Fourier modes and vary the Chebyshev points. We see Figure 4.6(b) that the stability regions will not change when the Chebyshev points is equal to 10 or more, although we believe if we add more grid points in space, we can find more resonance tongues.

After obtaining these convergence results, we compare the stability properties using 15 Fourier modes and 15 Chebyshev points to those obtained using separation of method (50 eigenvalues). Figure 4.6(c) shows that these two methods compute the same stability regions.

We mentioned in section 4.3 that if the slope of ε/δ is large, the ponytail is more likely to be unstable. Figure 4.6(c) also shows two lines corresponding to walking and running. When people are walking, the slope of $\varepsilon/\delta = (0.8 \times (4\pi)^2)/980 = 0.13$ and when people are running, the slope of $\varepsilon/\delta = (5.5 \times (6\pi)^2)/980 = 1.99$ (these values are same as in section 4.3). It is clear that the blue line lies fully in the unstable region, while the red line does not. However, as we mentioned, the flexible string may have an infinite number of tiny resonance tongues, which means when we treat ponytail as the flexible string, it is very unlikely to have stable regions for

the ponytail motion for different stride rates. Therefore, the ponytail will be unstable in lateral direction when people are running and is unlikely to be stable when people are walking. In conclusion, if we treat the ponytail as a flexible string, it has a high probability of being unstable.

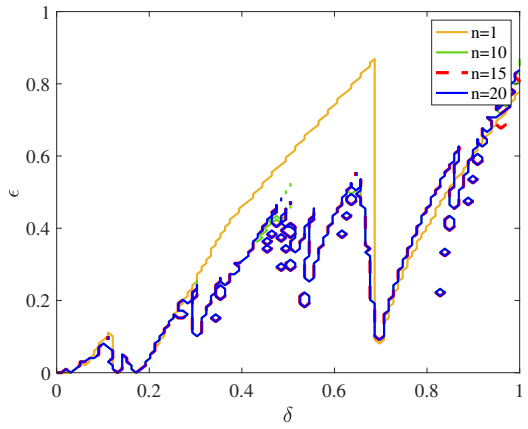

(a) 1, 10, 15 , 20 Fourier modes.

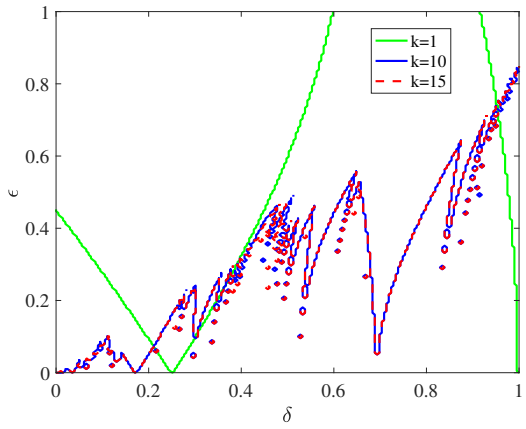

(b) 1, 10, 15 Chebyshev points.

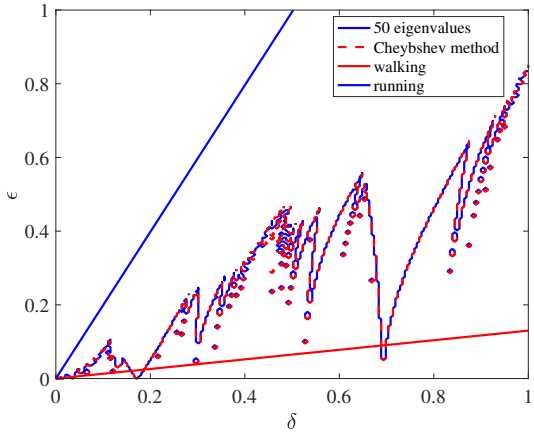

(c) The boundaries of the two methods

Figure 4.6: Figure (a) and (b) show the numbers of Chebyshev points and Fourier modes needed for accuracy, and Figrue (c) compare the boundary of the two methods.

Chapter 5

The rod problem

In this chapter, we consider the case of a flexible rod. As mentioned in Chapter 4, the method of separation of variables is not applicable in the flexible rod case. Hence this problem cannot be treated as an eigenvalue problem and can only be treated as a partial differential equation so as to discretize the equation (2.9) and find the stability regions.

5.1 Stability of the flexible rod

As mentioned in chapter 4, the Floquet Spectral method is much faster than the Floquet Monodromy matrix method and has the same accuracy, so we use the Floquet Spectral method to solve this problem in this chapter.

As for the flexible string problem, we use Fourier series to transform equation (2.9) to

$$-\sum_{n=-\infty}^{\infty} n^2 - (\delta + \varepsilon\cos t)([(1-s)\sum_{n=-\infty}^{\infty} X_n'(s)e^{int}]_s - \delta B\sum_{n=-\infty}^{\infty} X_n'''(s)e^{int}) + \mu((2in+\nu)\sum_{n=-\infty}^{\infty} X_n(s)) + \mu^2\sum_{n=-\infty}^{\infty} X_n(s) = 0 \tag{5.1}$$

Then we use the Chebyshev Spectral method to discretize in space.

We need to examine convergence before analyzing the stability region of flexible rod. We use $B = 0.01$ as an example to find the number of Chebyshev points and Fourier modes the we

need. The computational domain is 1×1, and 200 points in both δ and ε directions.

In Figure 5.1 (a), when we set Chebyshev points equal to 15, and we vary the Fourier modes from 5 to 15, we can find that 10 Fourier modes is accurate enough. Also, in figure 5.1 (b)when we set Fourier modes equal to 10, and vary the Chebyshev points from 10 to 20, we can find that when Chebyshev points equal to 15 is accurate enough to represent the boundary.

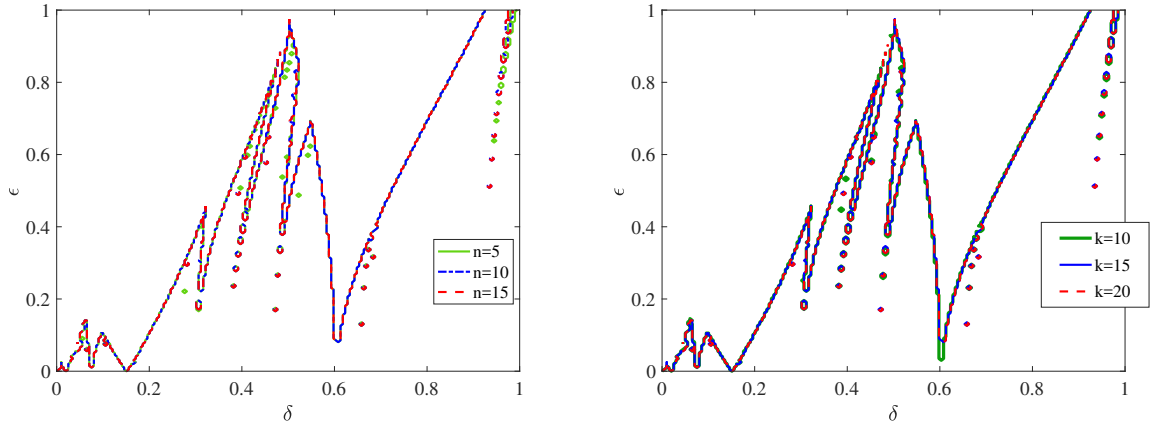

(a) Comparsion of the results in different Fourier modes when Chebyshev points =15.

(b) Comparison of the results in different Chebyshev points when Fourier modes =10.

Figure 5.1: Getting the converged solution of flexible rod when $B = 0.01$.

However, the flexible rod problem is no longer a fourth-order problem when $\delta = 0$ and the bending stiffness term vanishes, so we need to use the boundary conditions for the string in that ase.

After we get the converged solution, we need to discuss the impact of B for stability regions. We see from Figure 5.2 clear differences as B changes. As B becomes smaller, there are more unstable regions. The physical meaning is reasonable that when the bending stiffness is smaller, the ponytail will be more likely to become unstable and swing in the lateral direction.

We then compare the result for the flexible string with those for the flexible rod when B=0.01 and B=10^{-6} (see Figure 5.2). When B=10^{-6}, we take 15 Chebyshev points and Fourier modes, as the flexible string case in chapter 4. This is because as B becomes much smaller, the

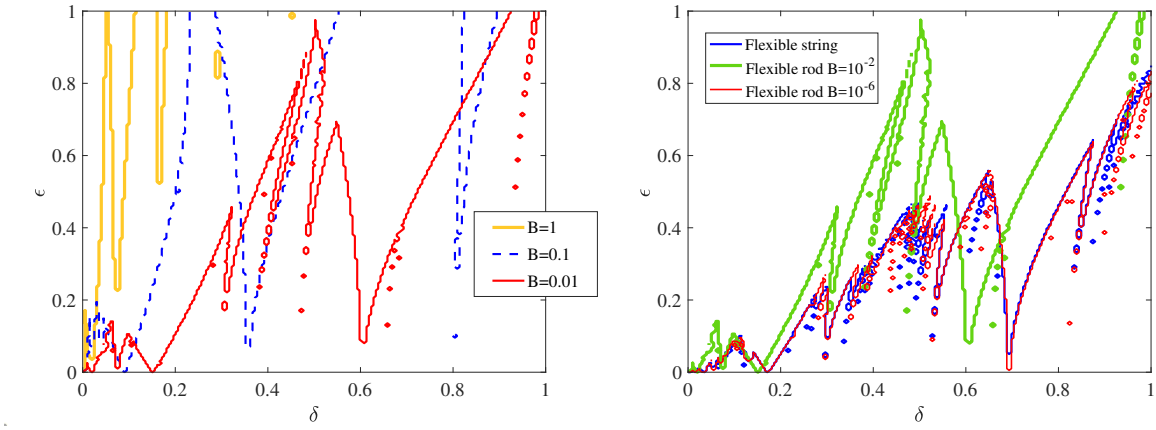

(a) Comparion of stability regions when B=1,0.1 and 0.01.

(b) Comparsion of Flexible string and Flexible rod when B=10^{-2} and B=10^{-6}.

Figure 5.2: Comparsion of stability regions of Flexible rod with different bending stiffness.

physical system becomes closer to the flexible string, which has an infinite number of resonance tongues and can not get the exact Chebyshev or Fourier modes to get converged result.

It can be seen from the Figure that when B becomes small, the stability regions of flexible rod look very similar to flexible string. The number and location of the resonance tongues become more and more similar to the string case as B decreases. Hence for very small B, the ponytail is unlikely to be stable.

5.2 Comparison to the Indian rope trick

We next fix the value of δ, and compare our results to those of Champneys and Fraser (their Figure 7)[2].

We recalculate their case and using the Floquet Spectral methods, and set $\delta = 0.1$ and a computational domain of 0.25×0.13 with 200 points in both δ and ε directions. Figure 5.3(a) shows the result of the Indian rope trick. The results are different from those of Champneys and Fraser. They restrict themselves to the Floquet multipliers equal to $+1$ or -1 (synchronous and subharmonic disturbances respectively) to find stability regions, which appears to be true.

However, they do not show the stability regions between stability boundaries we have in the lower right corner in Figure 5.3(a).

Figure 5.3(b) shows the result for ponytail motion. It confirms that that Indian rope trick is unstable when it is unforced and B is smaller than 0.13, while the ponytail is always stable. Another difference is that when the Indian rope trick is forced, unstable regions gradually become stable, but the stable regions of the ponytail become unstable after being forced. The only common thing for these two case is that when B is smaller and they are forced, there are more unstable regions.

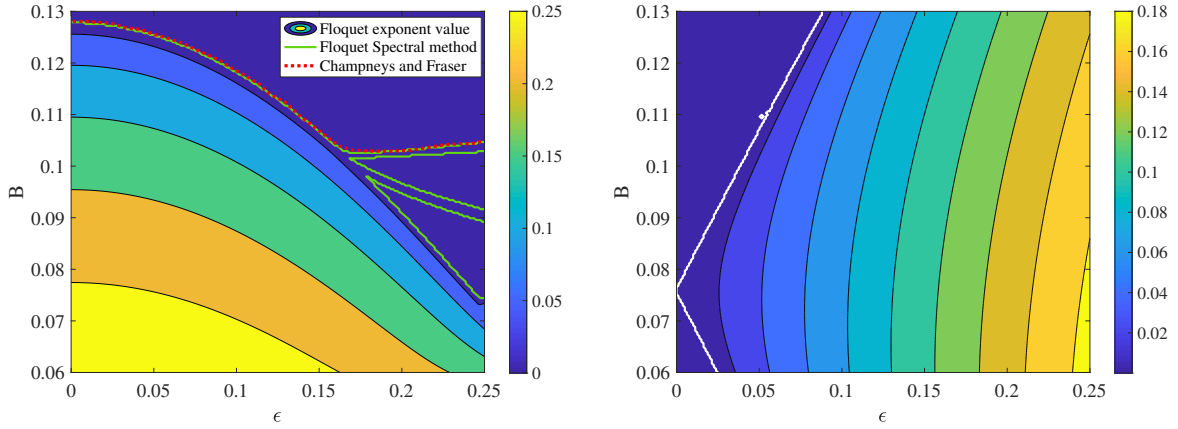

(a) Stability regions of Indian rope trick.

(b) Stability regions of ponytail.

Figure 5.3: Comparsion of stability regions when $\delta = 0.1$ in two cases

Chapter 6

The damped problem

6.1 The flexible rod with damping

In practical situations, the energy of flexible rod vibration will gradually be converted to heat or sound. This is damping. There are two types of damping: viscous damping and structural damping. Structural damping includes material damping and Coulomb or Dry-Friction Damping[9]. For our case, we consider viscous damping and material damping.

For viscous damping, when the ponytail vibrates in the air, the resistance offered by the air to the ponytail causes energy to be dissipated. For small oscillations (Reynolds number really), the viscous damping force is proportional to the velocity of the vibrating body, which is νx_t, and equation (2.9) can be rewritten as

$$x_{tt} + \nu x_t = (\delta + \varepsilon a_{tt})[(1-s)x_s]_s - \delta B_{ssss}, \tag{6.1}$$

where $\nu = \nu^*/(\rho\omega)$ is the dimensionless damping coefficient. This is the generic form for linear damping. In order to differentiate with the material viscous term (which will be discussed below), here we rename this type of damping linear damping in the following contents.

As the Floquet Spectral method is more efficient, this chapter we still use this method to

solve the problem, and look the values of Floquet exponents to find the stability regions.

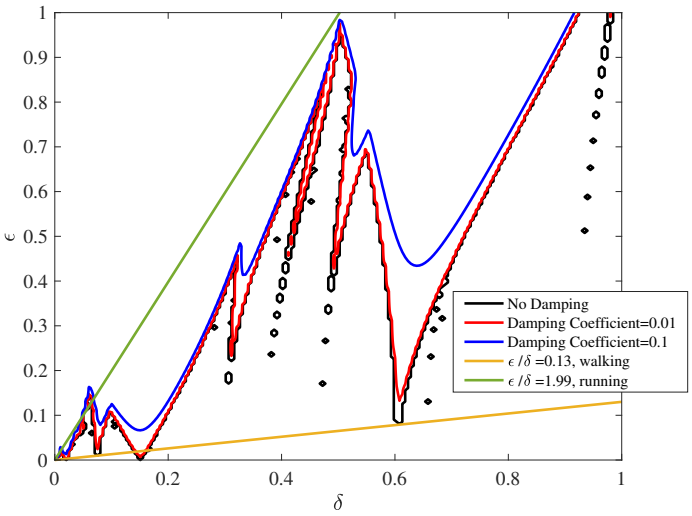

Figure 6.1: Comparsion of stability regions with undamped case when damping coefficient=0.1 and 0.01.

In Figure 6.1, we still use $B = 0.01$ as an example value, and when we choose the linear damping coefficient top be $\nu = 0.01$, 0.1 and 1. The results show that the linear damping is effective in transforming the resonance tongues from unstable to stable. When the value of linear damping coefficient becomes larger, this effect will grow larger. However, regions which are not close to the resonance points do not have much changes in the stability regions. Again, we use the line with ε/δ to help to find the stability of ponytail when people are walking and running. As ε/δ is small when people is walking, and this orange line is very close to the resonance points, this viscous damping can be really helpful to reduce the ponytail sway in lateral direction. However, when people is running, as the green line is not as close as the orange line to these resonance points, linear damping does not help to reduce the ponytail sway when people is running.

In order to help to reduce ponytail sway in lateral direction in the latter case, we need to consider other sorts of damping. The next step is to consider linear damping and material damping together, and the results are quite different.

Here we assume the material is a Kelvin–Voigt material, and we assume a stress relation

of the following form:

$$\tau = \sigma(x_s) + \eta x_{st} \tag{6.2}$$

where $\sigma(x_s)$ is the stress caused by a purely elastic spring with $\sigma(x_s) = Ex_s$, and E is the elastic modulus of material. Here ηx_{st} is the stress caused by a purely viscous damper, η is the viscosity coefficient of material, and this term could reflect the past history of the strain x_s[10]. It can also be treated as a lateral force acting on the beam which is negatively proportional to the bending rate[11].

Therefore, we add these terms to the equation of (2.10) as follows:

$$x_{tt} + \nu x_t = (\delta + \varepsilon a_{tt})[(1-s)x_s]_s - \delta B_{ssss} + Ex_{ss} + \eta x_{sts}, \tag{6.3}$$

where $E = E^*/(\rho L^2 \omega^2)$ and $\eta = \eta^*/(\rho L^2 \omega)$ are the dimensionless damping coefficients.

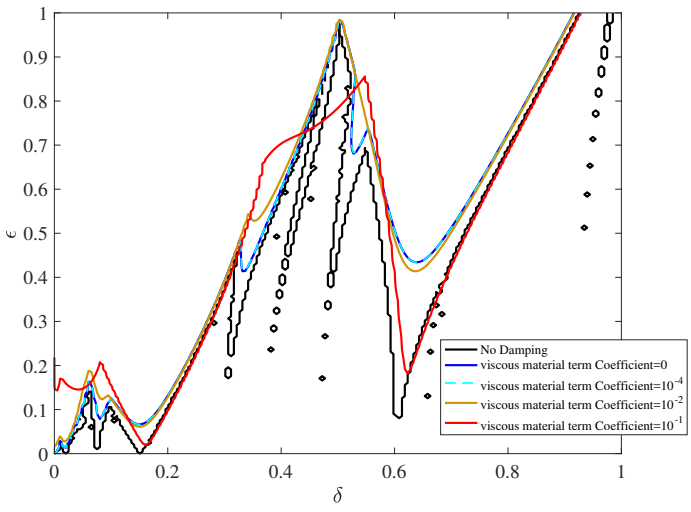

Figure 6.2: Comparsion of stability regions when linear damping coefficient is 0.1, material elastic modulus coefficient is 0, and material viscous damping coefficient is from 10^{-4} to 10^{-1}.

Firstly, we want to see the effects of material viscous damping term, so we set material elastic damping term equals to zero, set linear damping coefficient equals to 0.1 (as it has largest damping effect in figure 5.1), and vary the material viscous damping coefficient from 10^{-4} to

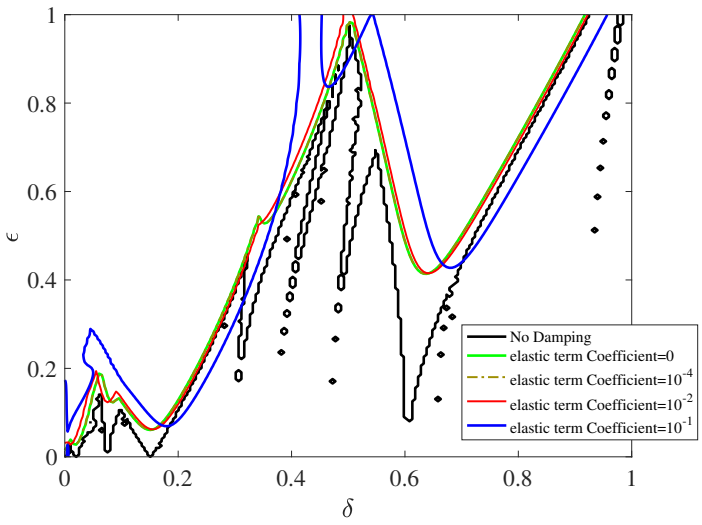

Figure 6.3: Comparsion of stability regions when linear damping coefficient is 0.1, material viscous damping coefficient is 10^{-2}, and material elastic modulus coefficient is from 10^{-4} to 10^{-1}.

10^{-1}. Figure 6.3 shows the result. We see that this material viscous damping does not reduce instability near near $\delta = 0.2$ and $\delta = 0.6$, and in fact makes some stable regions unstable. It only seems effective when the resonance tongue is relative tiny. Hence we investigate the effects of the material elastic damping term, as coefficient of material viscous damping term $= 10^{-2}$ relatively has a better effect, we set this term as this value, and linear damping coefficient still equals to 0.1. Figure 6.4 shows the result of varying the material elastic damping coefficient from 10^{-4} to 10^{-1}. After adding this type of damping, the stability region moves parallel from left to right. Hence this type of damping can affect the stability regions.

Therefore, this material damping is useful for tiny resonance tongues and can help move unstable regions. However, it still cannot help ponytail stability much e when people is running.

6.2 Comparison to the Indian rope trick

We use figure 5.3 as the basis of this damping study (fix $\delta = 0.1$), and figure 6.4 shows the result after adding viscous damping and material damping.

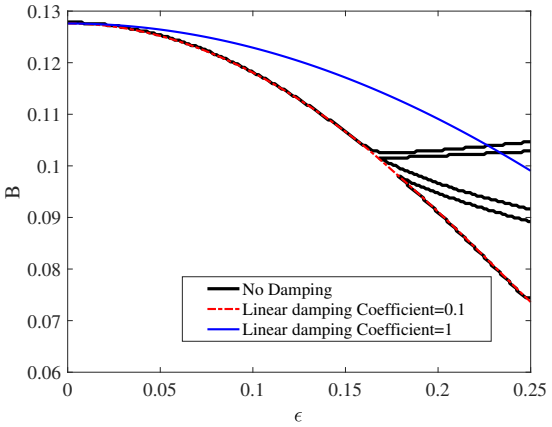

(a) Indian rope trick with linear damping.

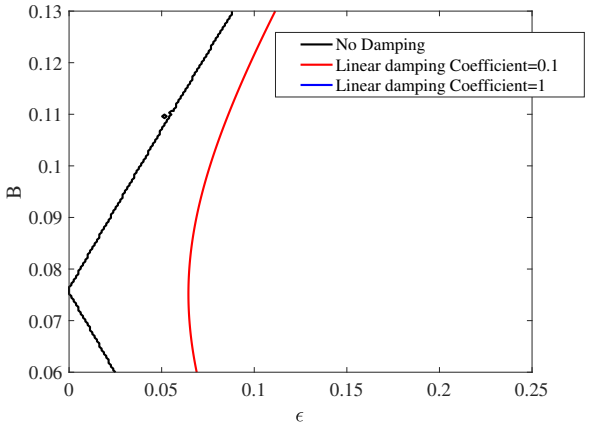

(b) ponytail with linear damping.

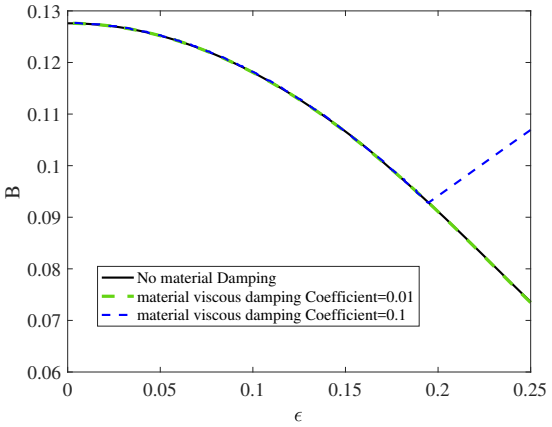

(c) Adding material viscous damping term to figure 6.4(a).

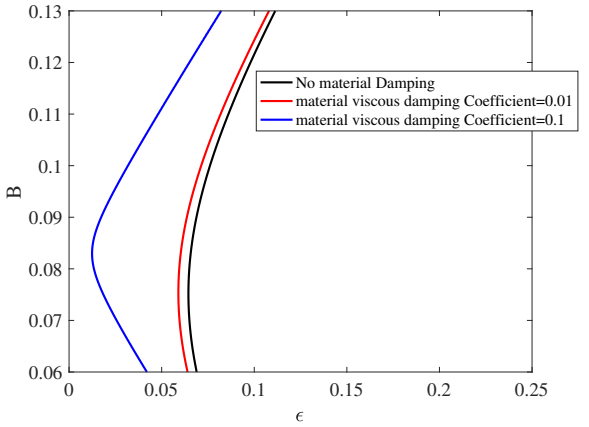

(d) Adding material viscous damping term to figure 6.4(b).

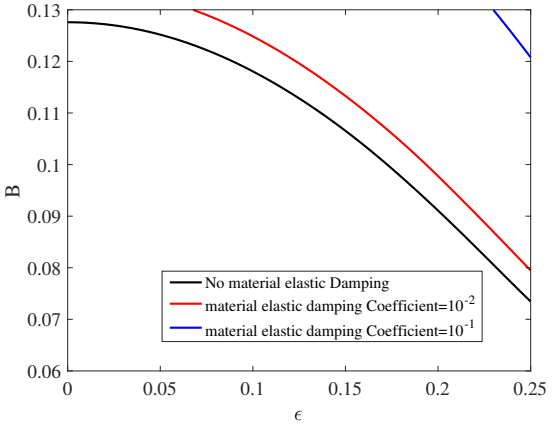

(e) Adding material elastic damping term to figure 6.4(c)..

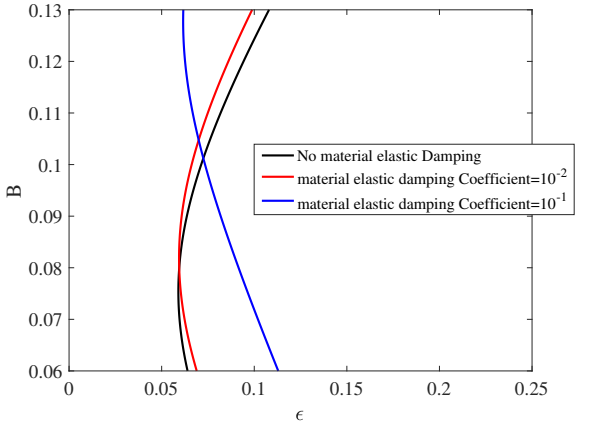

(f) Adding material elastic damping term to figure 6.4(d).

Figure 6.4: Comparsion of stability regions of Indian rope trick with ponytail when adding different types of damping.

For the Indian rope trick, we see from Figures 6.4(a), (c) and (e), that no matter what types of damping are added, the stable regions will become unstable, and this effect will grow larger when the damping coefficient is larger. This is reasonable as the Indian rope trick can only be stable when it is forced, and if this energy is dissipated by damping effects, the stable regions will become unstable.

For our ponytail case, the results look more interesting. Linear damping can help some regions with big resonance tongues to become stable (figure 6.4(b)), and adding material viscous damping term let stable regions become unstable again(figure 6.4(d)). Linear viscous damping and material viscous damping show the same effect as we discussed in section 6.1, but the result of adding material elastic damping (figure 6.4(f)) is not clear.

Therefore, for our ponytail case, linear damping is very good for regions which have large resonance damping, and material viscous damping does bad for these regions. And material elastic damping is good to move stability regions, and this damping term seems to be useful in industry if some types of machine do not want some fragile place to have large resonance regions, this type of damping is helpful.

Chapter 7

Conclusion

This thesis has used Floquet theory to find the stability regions of ponytail motion. A Chebyshev Spectral method has been used to discretize the equations in space and Fourier series or Runge-Kutta method has been used to discretize in time, corresponding to the Floquet spectral method and the monodromy method respectively.

We separately analyze unforced flexible rod problem, forced flexible string problem, forced flexible rod problem and damped problem of forced flexible rod. The main result as follows. The unforced flexible rod and forced flexible string problems can use the method of separation of variables. However, the forced flexible rod problem requires the Chebyshev Spectral method to discretize in space. For the unforced problem, the method of separation of variables turns the problem into an eigenvalue problem, showing that there is no unstable regions, which means ponytail will not sway in lateral direction without external forcing. For the forced flexible string problem, we have described the Floquet Spectral method and Floquet monodromy matrix method used to solve the problem. Sections 4.1 and 4.3 show how to solve using the method of separation of variables, and use the points $\lambda_n(\delta,\varepsilon)$ to find whether the ponytail is stable in lateral direction as a function of stride rate. To verify its accuracy this method has been compared with equation (4.1) discretized both in time and space. For the forced flexible rod problem, we

have discussed the bending stiffness effect to the stability regions. Sections 5.1 and 5.2 show the results compared with the flexible string problem for different value of bending stiffness, and the result compared with Champneys'. For the damping problem, linear damping and Kelvin–Voigt damping have been used to decay energy of ponytail motion to turn the instability regions to be stable, and the effects of linear damping is more reasonable and useful than Kelvin–Voigt damping.

This thesis is co-authored with Dingqian Ding, Stefan G. Llewellyn Smith and Todd Christopher. The thesis author is the primary investigator and author of this material.

Bibliography

[1] Raymond H. Plaut and Lawrence N. Virgin. Pendulum models of ponytail motion during walking and running. *Journal of Sound and Vibration*, 332(16):3768 – 3780, 2013.

[2] Alan R. Champneys and W. Barrie Fraser. The "Indian rope trick" for a parametrically excited flexible rod: linearized analysis. *Proceedings of the Royal Society of London. Series A: Mathematical, Physical and Engineering Sciences*, 456(1995):553–570, Mar 2000.

[3] Joseph B. Keller. Ponytail motion. *SIAM Journal on Applied Mathematics*, 70(7):2667–2672, 2010.

[4] Ö. Turhan. A generalized Bolotin's method for stability limit determination of parametrically excited systems. *Journal of Sound and Vibration*, 216(5):851 – 863, 1998.

[5] Alexander P. Seyranian. Parametric resonance in mechanics: Classical problems and new results. *Journal of System Design and Dynamics*, 2(3):664–683, 2008.

[6] Lloyd N. Trefethen. *Spectral Methods in MATLAB*. Society for Industrial and Applied Mathematics, 2000.

[7] R2019a documentation, 2019.

[8] Masahiro Takahashi, Haruko Hoshikawa, Naomi Tsujita, and Ikuyo Akiyama. Effect of labyrinthine dysfunction upon head oscillation and gaze during stepping and running. *Acta Oto-Laryngologica*, 106(5-6):348–353, Jan 1988.

[9] Singiresu S. Rao. *Mechanical Vibrations*. Fifth edition, 2011.

[10] James M. Greenberg, Richard C. Mac Camy, and Victor J. Mizel. On the existence uniqueness and stability of solutions of the equation $\sigma(u_x)u_{xx} + \lambda u_{xtx} = \rho_0 u_{tt}$. *Journal of Mathematics and Mechanics*, 17(7):707–728, 1968.

[11] David L. Russell. *4. On Mathematical Models for the Elastic Beam with Frequency-Proportional Damping*, pages 125–169.